2016-12

Failure Loading of Metallic and Composite Cylinders Under Internal Pressure Loading

Kwon, Y.W.

Journal of Pressure Vessel Technology December 2016, Vol. 138.
http://hdl.handle.net/10945/50356

Failure Loading of Metallic and Composite Cylinders Under Internal Pressure Loading

Y. W. Kwon
Department of Mechanical and Aerospace Engineering, Naval Postgraduate School, Monterey, CA 93943

T. Ponshock
Department of Mechanical and Aerospace Engineering, Naval Postgraduate School, Monterey, CA 93943

J. D. Molitoris
Lawrence Livermore National Laboratory, Livermore, CA 94551

A new mechanical device was developed to apply internal pressure loading to a cylindrical structure in order to determine its failure strength and failure mode under pressure loading. The device can be used for a uniaxial testing machine to apply internal pressure to a cylindrical structure. As a result, the developed device does not require any fluid to generate internal pressure loading. The device consists of two truncated conical shape of rams and eight pieces of the identical shape of wedges. The effectiveness of the device was assessed using both detailed finite element analyses of metallic cylinders as well as the analytical analysis. Then, a set of experimental tests were undertaken for aluminum alloy cylinders in order to evaluate experimental failure strength against the numerical and analytical results. Finally, composite cylinders made of glass-fiber or carbon-fiber woven fabrics were tested using the device, and the experimental results were compared to the predicted results using a multiscale analysis model. Those results agreed well with each other. [DOI: 10.1115/1.4033772]

Keywords: mechanical device for internal pressure loading, failure of cylindrical structure, composite materials, multiscale analysis

1 Introduction

Because of multiple benefits such as high specific strength and stiffness, composite materials have gradually replaced traditional metallic materials in many applications. One of such cases is composite pressure vessels and pipes which are subjected to high internal pressure loading. In order to design a pressure vessel or pipe subjected to internal pressure, it is necessary to predict its burst pressure. Otherwise, an experimental test should be conducted to determine the burst pressure.

There has been extensive prior work on both the analytic and experimental analysis of composite pressure vessels and pipes [1–5]. Research conducted in Ref. [1,2] determined an elastic solution for the burst pressure of thick-walled composite pressure vessels with an internal pressure. Xing et al. [3] examined the effects of various filament-winding angles to optimize composite filament-wound pressure vessel properties and found an optimum winding angle for the carbon-fiber composite (CFC) and glass-fiber composite (GFC) cylinders. On the other hand, Hwang et al. [4] investigated a new approach for evaluating the material properties of filament-wound composite vessels.

With the exception of the research in Ref. [4], most of the existing research used the current standard test methods including the unidirectional plate test (ASTM D3039), split-disk method (ASTM D2290), and the hydraulic pressure test of filament-wound pressure vessels (ASTM D2585). For the testing of open-ended composite cylinders, all of these test methods have shortcomings. The unidirectional plate test uses fiber filaments wound around a flat plate mandrel to fabricate the test specimen, and errors are introduced due to varying geometry and residual stresses compared to the actual cylinder. On the other hand, the split-ring method introduces errors due to loading not being purely tensile during the test [6]. Although the hydraulic pressure test gives excellent results for pressure vessels, the composite cylinders testing would require capping the ends to allow pressurization from an external source.

Horide et al. [5] successfully tested multi-ply GFC cylinders under internal pressure using a modified ring burst test that removed much of the errors seen with ASTM D2290. However, their test method requires a thin composite ring similar to the ASTM split-ring specimen for testing. There are some new designs for applying internal pressure to a cylinder [6–8]. All devices are similar in that they require a fluid to pressurize the test cylinder using either a high-pressure hydraulic pump or through application of a compressive force to a piston. These designs essentially cap the ends of the cylinder and require complex equipment to conduct testing.

The objective of this research is the development of a purely mechanical device capable of testing hollow cylinders to failure without modification to the cylinder. Data recorded during the tests allow for directly determining the material properties and burst pressure of the cylinder. This test device is used for aluminum cylinders to determine its effectiveness. Then, the device is applied to composite cylinders to determine their burst pressure. Finally, a multiscale analysis technique is used to predict the effective modulus and the burst pressure of the cylinders.

Section 2 describes the mechanical test device used for the present study. Then, a fabrication technique for composite cylinders is presented. Section 4 provides the description of the multiscale analysis technique followed by test results and discussion. Finally, conclusions are presented.

2 Description of Experimental Apparatus

A mechanical testing device was designed and fabricated in order to apply internal pressure loading to a hollow cylinder. The device can be used with a uniaxial testing machine, and it does not require any fluid to generate internal pressure loading. The device consists of two main parts as sketched in Fig. 1. The first part comprises two truncated conical rams at the top and bottom, which move in the axial direction. The second main part comprises eight identical conical wedges which move in the radial direction. All wedges have arc shapes of the subtended angle 45 deg. Figure 1(*b*) shows the wedges. Because all wedges were manufactured from one cylindrical piece using the electrical discharging machining technique, there is a very small gap between

Contributed by the Pressure Vessel and Piping Division of ASME for publication in the JOURNAL OF PRESSURE VESSEL TECHNOLOGY. Manuscript received January 15, 2016; final manuscript received May 27, 2016; published online July 18, 2016. Assoc. Editor: Pierre Mertiny.

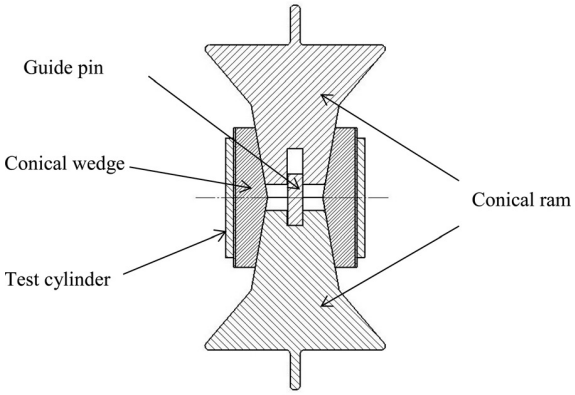

(*a*)

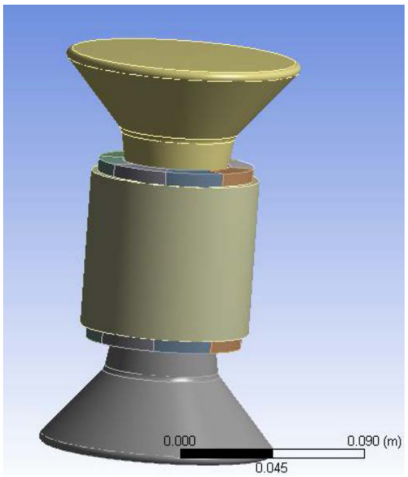

(*b*)

Fig. 1 Mechanical testing device to apply internal pressure: (*a*) cross-sectional view and (*b*) three-dimensional view

any two neighboring wedges. As a result, the wedges can fit inside the cylinders even though the outer diameter of the wedge and the inner diameter of the cylinder have the same diameters. During the experiment, both rams are inserted into the wedges such that the wedges and the cylinder have the initial contact. Then, the ram force is applied from that point. As the conical rams move axially, the wedges move radially resulting in internal pressure to the surrounding cylinder. A guide pin is used to align the rams during its motion. Both rams and wedges are made of high strength and high stiffness materials as compared to the cylinder material so that the device may have a minimal deformation without yielding during the operation. For the present study, 17-4 PH stainless steel was selected for the conical rams and wedges.

In order to evaluate the performance of the device, computer modeling and simulation was conducted using the finite element method (FEM). Then, the analytical solutions were developed and compared to the FEM results. Figure 2 shows the representative finite element mesh of the mechanical device and the cylinder under consideration. With a mesh sensitivity study, a much refined mesh was used for the study. However, the mesh is so dense and it cannot be seen clearly. As a result, a coarse mesh is shown in Fig. 2 for visual clarity of the mesh. The actual mesh has more than 300 elements along the circumference.

Even though one-eighth model could be used, the whole body was modeled because the computation was still quite fast. There were a couple of contact surfaces in the model. One is the sliding interface between the wedges and the conical rams. This was modeled as a frictional sliding contact surface. The other contact lies between the wedges and the inner surface of the cylinder.

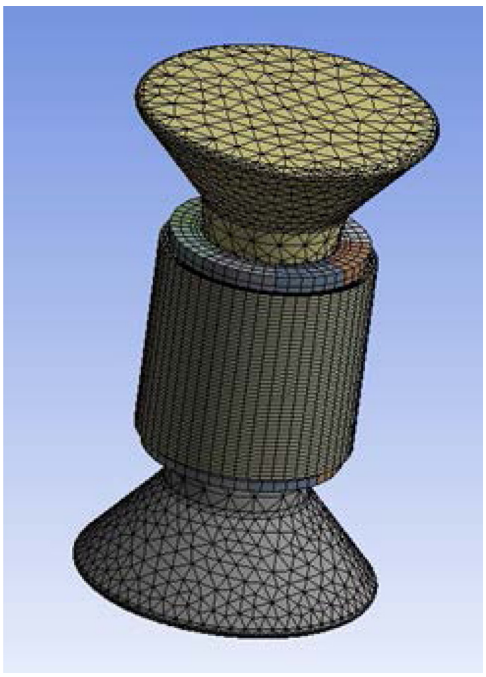

Fig. 2 Finite element meth of the mechanical device and aluminum cylinder

Because the wedges and the cylinder move together virtually, the relative motion is almost negligible. As a result, any frictional contact model is acceptable. To make the whole FEM model simple, the same contact model was applied to both contact faces of the ram/wedge and the wedge/cylinder. On the other hand, there is a very tiny gap between two neighboring wedges. Because they do not contact during deformation, no contact surface is necessary among wedges.

The selected material for the cylinder was the aluminum alloy 6061. All the material properties used in the simulation are listed in Table 1. The cylinder has the internal diameter 76.2 mm (3.0 in.) and the wall thickness 3.175 mm (0.125 in.). The cylinder length is also 76.2 mm (3.0 in.). The elastoplastic analysis was conducted for the aluminum cylinder because the internal loading was applied much beyond the elastic limit.

As the device applies internal pressure loading to a cylinder, the eight wedges start to result in a very small gap between two neighboring wedges. As a result, the pressure loading to the cylinder becomes nonuniform at the gap locations. To check such nonuniformity of the load, the hoop strain is plotted across the circumferential direction of the cylinder which is pushed out by the wedges. Each wedge has an arc shape of the subtended angle of 45 deg. As a result, the hoop strain variation is plotted along the cylinder corresponding to the subtended angle of one wedge because of the periodic symmetry of the strain. Figure 3 shows that the hoop strain is quite uniform at the location between 5 deg and 40 deg. Because the angle in Fig. 3 was measured from one end of the wedge to the other, the angles near 0 deg and 45 deg

Table 1 Material properties used in FEM models

Material	17-4 PH stainless steel	Aluminum alloy 6061-T6
Elastic modulus	200 GPa	68.9 GPa
Poisson's ratio	0.28	0.33
Yield strength	1.219 GPa	276 MPa
Tangential modulus	N/A[a]	500 MPa
Ultimate strength	N/A[a]	310

[a]The stress level never went beyond yield strength.

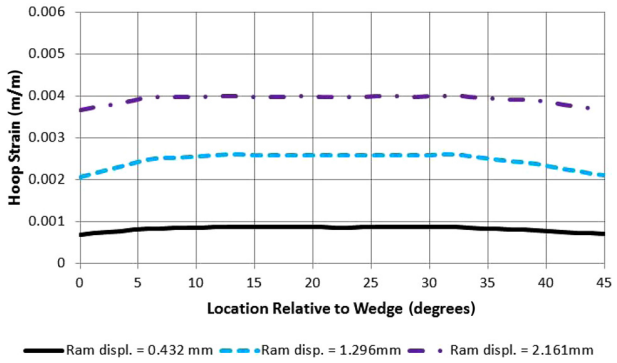

Fig. 3 Plot of FEA hoop strain variation along the arc of each wedge for three different target hoop strains

represent the locations close to the gap between two neighboring wedges. As expected, the hoop strains at the gap locations are smaller than the other locations. Because failure would occur at the larger strain location, the numerical results at the midsection of each wedge are of interest and compared to the analytical solution which does not consider a gap in wedges.

The analytical solution is obtained as below for linear elastic deformation. First of all, the equilibrium of force of the truncated conical shape of ramp along the axial direction is obtained from the free-body diagram as shown in Fig. 4(*a*)

$$F = N\cos\theta + f\sin\theta \tag{1}$$

where all the forces in the free-body diagram are the resultant forces applied to the corresponding surface areas. Use of Coulomb's friction law states $f = \mu N$, where μ is the coefficient of friction. Similarly, the force equilibrium in the radial direction of a wedge gives

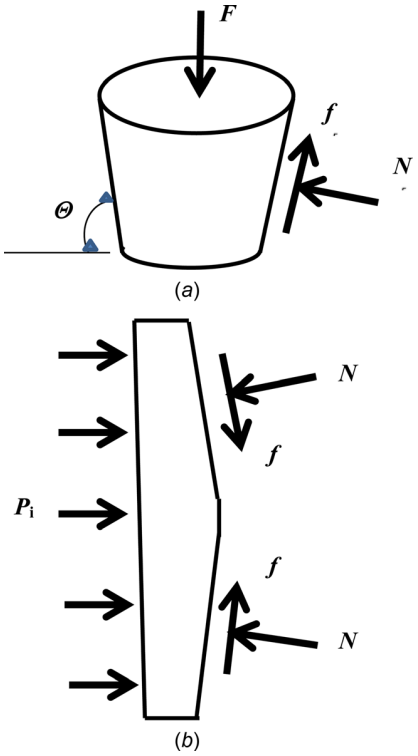

Fig. 4 Free-body diagrams: (*a*) ram and (*b*) wedge

$$p_i(\pi aL) = N\sin\theta - f\cos\theta \tag{2}$$

Here, p_i is the internal pressure, and L and a are the length and inner radius of the cylinder. Combining the two equations yields

$$p_i = \frac{F}{\pi aL}\left(\frac{\tan\theta - \mu}{1 + \mu\tan\theta}\right) \tag{3}$$

For an axisymmetric cylinder, the hoop strain at the outer surface of the cylinder is expressed as

$$\varepsilon_h^o = \frac{2a^2 p_i}{E(b^2 - a^2)} \tag{4}$$

where a, b, and E are the inner radius, outer radius, and the elastic modulus of the cylinder. For the inner surface of the cylinder, the hoop strain is

$$\varepsilon_h^i = \frac{a^2 p_i}{E(b^2 - a^2)}\left[(1-\nu) + (1+\nu)\frac{b^2}{a^2}\right] \tag{5}$$

Substitution of Eq. (3) into Eqs. (4) and (5) results in

$$\varepsilon_h^o = \frac{2aF}{\pi E(b^2 - a^2)L}\left(\frac{\tan\theta - \mu}{1 + \mu\tan\theta}\right) \tag{6}$$

and

$$\varepsilon_h^i = \frac{aF}{\pi E(b^2 - a^2)L}\left[(1-\nu) + (1+\nu)\frac{b^2}{a^2}\right]\left(\frac{\tan\theta - \mu}{1 + \mu\tan\theta}\right) \tag{7}$$

If the cylinder has a very small thickness compared to its radius, Eqs. (6) and (7) are simplified to

$$\varepsilon_h = \frac{F}{\pi ELt}\left(\frac{\tan\theta - \mu}{1 + \mu\tan\theta}\right) \tag{8}$$

where $t = b - a$ is the wall thickness. The hoop stress inside the cylinder is

$$\sigma_h^i = \frac{(a^2 + b^2)F}{\pi E(b^2 - a^2)aL}\left[\frac{\tan\theta - \mu}{1 + \mu\tan\theta}\right] \tag{9}$$

For a thin-walled cylinder, Eq. (9) is also simplified to

$$\sigma_h^i = \frac{F}{\pi EtL}\left[\frac{\tan\theta - \mu}{1 + \mu\tan\theta}\right] \tag{10}$$

The aluminum alloy cylinder discussed previously is considered as a thin-walled cylinder. As a result, Eq. (8) is compared to the FEM results with different values for the coefficient of friction in Table 2. The angle $\theta = 80$ deg was used in this study, and the deformations are linear elastic for the applied load. The maximum FEM hoop strains were selected, which occur inside the cylinder at the locations away from the wedge gaps. Both analytical and FEM results compare very well. Therefore, even though the FEM model consists of eight pieces of wedges with discontinuity, the resultant maximum hoop strains in the cylinder at the location of the

Table 2 Comparison hoop strains between FEM and analytical solution of the device

Force applied to ram (kN)	Coefficient of friction	FEM hoop strain	Analytical hoop strain	% error based on analytical
10	0.01	1.02×10^{-3}	9.93×10^{-4}	2.72
10	0.05	8.25×10^{-4}	8.11×10^{-4}	1.73
10	0.1	6.59×10^{-4}	6.59×10^{-4}	0.00

Fig. 5 E-glass fiber (left) and carbon-fiber (right) composite cylinders

midsection of each wedge are very close to the analytical hoop strains with the uniform pressure assumption. This suggests that the proposed device is suitable to investigate failure of cylinder subjected to uniform internal pressure loading using a uniaxial testing machine.

3 Fabrication of Composite Cylinders

While aluminum alloy cylinders were ordered from a manufacturer and tested as received, composite cylinders were fabricated at the laboratory. Woven fabric composites were wrapped around a cylindrical mold. Before wrapping the composite layers over the mold, a layer of release ply paper followed by a layer of Teflon sheet was wrapped around the aluminum cylinder mold. The two layers prevent any epoxy from sticking to the form and ensuring an easy release following curing. Next, two rubber drain pipe couplers were used to create top and bottom guides for composite strip alignment as well as an outer surface form for the composite cylinders.

To begin layup, the epoxy was applied to either side of the first part of the strip as well as the mold rig. Next, the strip was hand-wrapped around the mold cylinder between the two rubber guides. Additional epoxy was applied between each layer of the wrap using the brush and spread evenly with the roller. The next step in fabrication was wrapping the composite cylinder with the pre-prepared strip of perforated release ply and breather cloth. A spiral-wound line connected to a vacuum pump was then taped to the mold cylinder. The entire mold cylinder was then removed from the base and wrapped in breather cloth to absorb excess resin and prevent the edges of the aluminum mold cylinder from cutting into the vacuum bag. Finally, the mold cylinder was placed in a vacuum bag and under 0.508–0.635 m hg vacuum for 1.25–1.5 hrs to allow the curing process to begin. Following the initial cure time, a roller was used to smooth the outer surface before placing the rubber outer form around the composite cylinder and wrapping tightly with electrical tape. The mold was then placed in a vacuum bag for additional 3 hrs under 0.508–0.635 m hg vacuum to allow for complete curing of the epoxy resin.

As a final step to create uniform cylinders, a rotary cutting tool was used to trim the top and bottom of each rough composite cylinder to create finished composite cylinders of 76.2 mm (3 in.) tall, with a 76.2 mm (3 in.) inside diameter for testing. Figure 5 shows the typical finished glass and carbon-fiber composite cylinders. The nominal wall thickness of the GFC cylinder is 5.5 mm while that of the CFC cylinder was 2.5 mm.

4 Multiscale Analysis of Composites

A multiscale model was used to predict the stiffness and strength of composite cylinders tested in this study. Because the cylinders were fabricated using plain weave woven fabrics, the multiscale analysis consists of the two main modules. The schematic drawing of the multiscale analysis is shown in Fig. 6. The multiscale analysis consists of two loops: forward process called "stiffness loop" and the backward process called "strength loop."

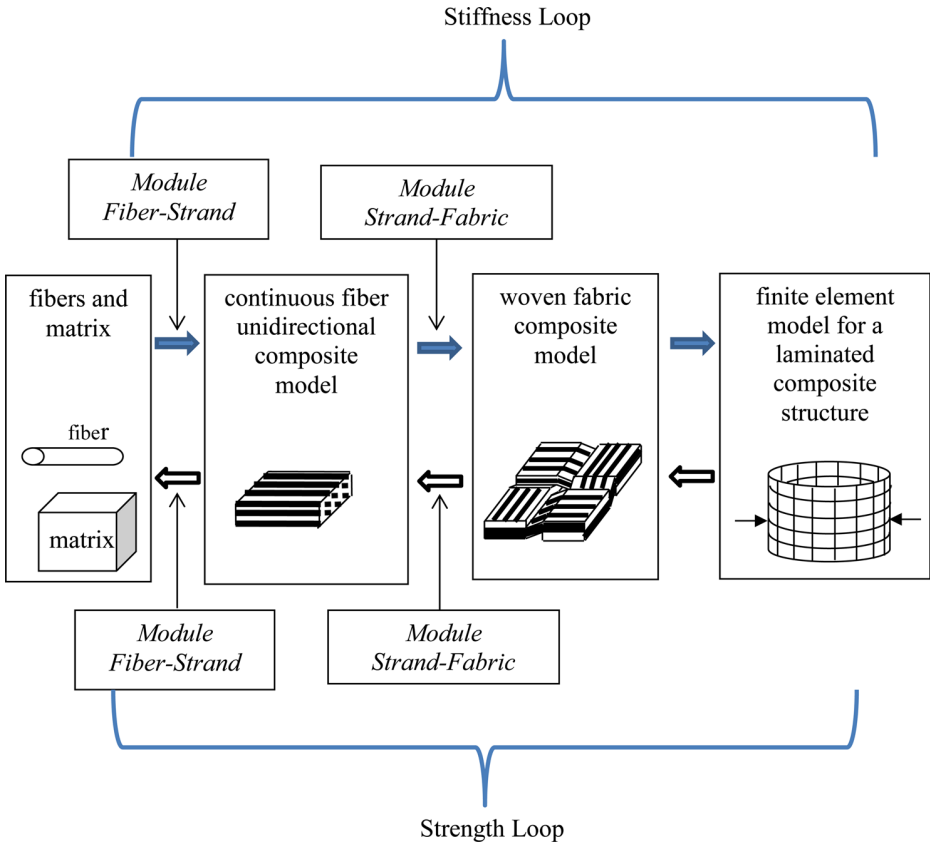

Fig. 6 Schematic of multiscale analysis of woven fabric composite structure

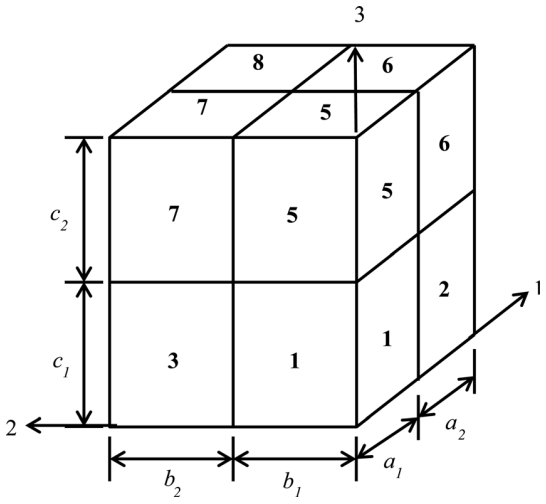

Fig. 7 Unit cell model for fibrous composite

The first module called "fiber-strand module" is first used to determine the effective material properties of the unidirectional composites made of fiber and matrix materials and their volume fraction. This is accomplished using a unit cell model as sketched in Fig. 7. Once the material properties of the unidirectional composites are determined, those properties are also used for the next module called "strand-fabric module" which eventually computes the effective material properties of the woven fabric composites using the geometric architectural data as shown in its unit cell in Fig. 8. Theses effective values are used for the finite element analysis of composite cylinders for applied loading or for an analytical solution if available. The finite element analysis (FEA) or the analytical solution results in stresses and strains in the composite cylinders. However, those values are the effective stresses and strains at the composite material level. Those stresses and strains are decomposed into the stresses and strains at the fiber and matrix level using the same modules used previously as shown in Fig. 6. For the present study, as the maximum fiber stress in the hoop direction reaches the tensile strength of the material, the cylinder is considered failed.

For the sake of brevity, details of the modules are not presented here. References [9–13] provide the details of the modules. Instead, some assumptions used in the modules are briefly stated in this section.

The unit cell models as shown in Fig. 7 or 8 are comprised of subcells. Each subcell can have a different material and the unit cell model can solve for equivalent composite moduli, Poisson's ratio, and coefficient of thermal expansion. Each subcell is assumed to have a uniform stress and strain state for mathematical simplicity. Then, stress equilibrium and strain compatibility among subcells are applied. Then, the total unit cell stresses and strains can be found by averaging the subcell stresses and strains based on subcell volume fractions. Mathematical operations of the equations stated above result in two final expressions. One is an expression to compute effective material properties of the unit cell from the subcell properties. The other is an expression to decompose the unit cell strains into subcell strains. Then, the subcell stresses can be computed from the subcell strains using the material properties of the corresponding subcell.

5 Experimental Results and Discussion

5.1 Aluminum Cylinders. First of all, the aluminum cylinders were tested to evaluate the test device as well as to compare their experimental results to previous FEA and analytical results. Strain gages were attached to the outer surfaces of all the cylinders to be tested. Multiple gages were attached to each cylinder along the hoop and axial directions. At least, one strain gage was attached at the cylinder location which was in contact with the middle of a wedge while one strain was attached to the cylinder location between two neighboring wedges. As shown in the FEA results, the reading from the former strain gage was expected to be greater than that from the latter strain gage.

Before testing, all the cylinders were measured for their geometry, and any geometric variation along the circumference of the cylinders was noted. The nominal geometry of the cylinders had the inner diameter 76.2 mm (3.0 in.), thickness 3.175 mm (0.125 in.), and length 76.2 mm (3.0 in.). The hoop and axial strains of three aluminum cylinders are plotted in Fig. 9. Because every cylinder had multiple strain gages, each strain in the plot is the average of all strains.

The section of the linear relationship between the applied force and strain in Fig. 10 was compared to the analytical expression (Eq. (8)). Then, the resultant frictional coefficient was calculated to be 0.12, and this value was used for the rest of the study to compute experimental pressure loading. The FEA results using the coefficient of friction 0.12 are compared to the experimental data in Fig. 10. They compare very well for the linear section which has elastic deformation before yielding.

Table 3 shows the load, pressure, and strains when three aluminum cylinders failed. They are quite consistent. The failure pressure is approximately 18 MPa with the failure hoop strain 0.0045. The experimental failure pressure is compared to both analytical and FEA failure pressure in Table 4. The analytical failure pressure was based on no strain hardening (i.e., perfectly plastic) assumption. The failure pressure was computed from

$$p_f = p_y \frac{2b^2}{b^2 - a^2} \ln \frac{b}{a} \tag{11}$$

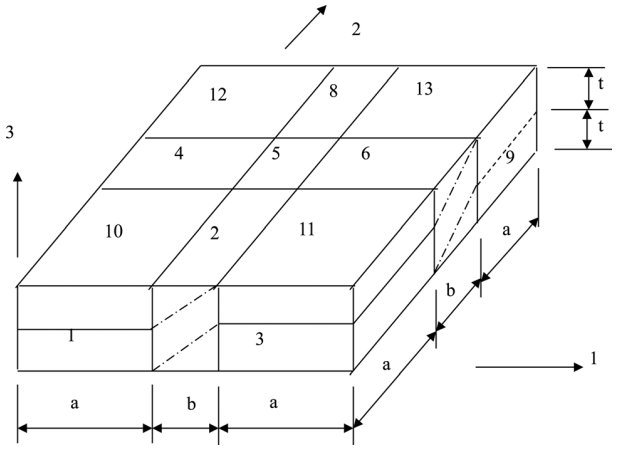

Fig. 8 Unit cell model for plain weave fabric composite

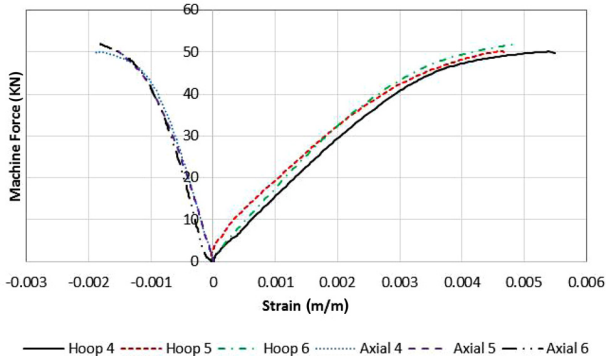

Fig. 9 Applied force versus strain for aluminum cylinders

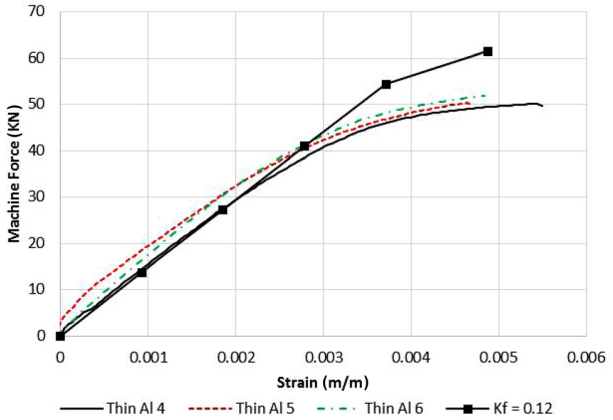

Fig. 10 Comparison of experimental and FEA results for aluminum cylinders using friction coefficient of 0.12

Table 3 Results for aluminum cylinders at failure

Sample	Force (kN)	Pressure[a] (MPa)	Hoop Strain	Axial Strain
Al cyl. #1	49.75	18.1	0.00550	−0.00189
Al cyl. #2	50.24	18.2	0.00468	−0.00155
Al cyl. #3	51.94	18.8	0.00483	−0.00181
Average	50.64	18.4	0.00500	−0.00175

[a]The pressure was computed from the force and the coefficient of friction using Eq. (3).

Table 4 Experimental, analytic, and FEA failure pressures for aluminum cylinders

	Average	Error (%)
Experimental failure pressure[a] (Pa)	1.84×10^7	—
Analytic failure pressure (Pa)	1.34×10^7	−27.1
FEA failure pressure (Pa)	2.27×10^7	23.7

[a]The pressure was computed from the force and the coefficient of friction using Eq. (3).

where p_f and p_y are the failure pressure and the pressure at which the cylinder begins yielding. Since the actual aluminum shows strain hardening, the analytical failure pressure underestimated the experimental value. On the other hand, the FEA solution assumed a linear hardening rule, and the failure pressure was determined when the equivalent stress inside the cylinder reached the ultimate strength of the aluminum alloy. The actual aluminum alloy has a nonlinear strain hardening behavior. The FEA overestimated the failure pressure compared to the experimental result. If a more accurate strain hardening curve were used in the FEA model, the predicted value would be much closer to the experimental value. However, that was not the objective of this study so that it was not attempted. A failed aluminum cylinder is shown in Fig. 11. The crack initiated at the top edge of the cylinder consistently and propagated along the longitudinal direction of the cylinder because the uniaxial test machine pushed the top side while the bottom was stationary. A finite element analysis confirmed that the stress was slightly larger at the free edge than the midsection of the cylinder. However, the difference was minimal. In addition, the failure along the longitudinal direction was almost simultaneous. On the other hand, composite cylinders also initiated failure at an uncontrollable defect site such as misalignment of fibers, nonuniform thickness of wall thickness, etc., even though the variations were small.

5.2 Composite Cylinders. Once the mechanical device was assessed using aluminum alloy cylinders, the device was used to determine the failure loading of composite cylinders which were constructed with glass-fiber or carbon-fiber woven fabric composites as described in Sec. 3. The composite cylinders had the same geometry as the previous aluminum alloy cylinders except for the thickness. The glass-fiber woven fabrics composite cylinders, called GFC cylinders from now on, had the wall thickness of 3.5 mm while the carbon-fiber woven fabrics composite cylinders, called CFC cylinders, had the wall thickness 2.5 mm. Both GFC and CFC cylinders had quasi-isotropic material properties because materials properties were the same in the fill and warp directions of the plain weave composite. As a result, the analytical equations presented previously can be also used for the composite cylinders.

Fig. 11 Failed aluminum cylinder

The next experiments were conducted for CFC cylinders. Before predicting the failure of the CFC cylinders, dog-bone shape CFC tensile coupons were tested to find out their material properties. Figure 12 shows the stress–strain curve of a CFC tensile coupon. The result shows that the effective elastic modulus of the CFC is 40 GPa, the failure strength is 500 MPa, and the fracture strain is 0.0135 m/m. For the multiscale analysis model, the following constituent material properties were used. The carbon

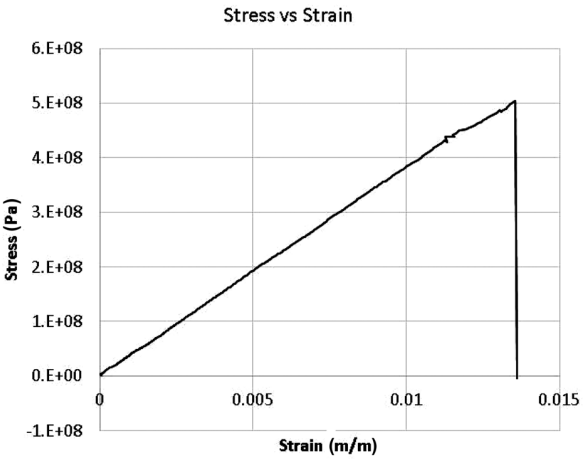

Fig. 12 Tensile stress–strain curve of CFC specimen

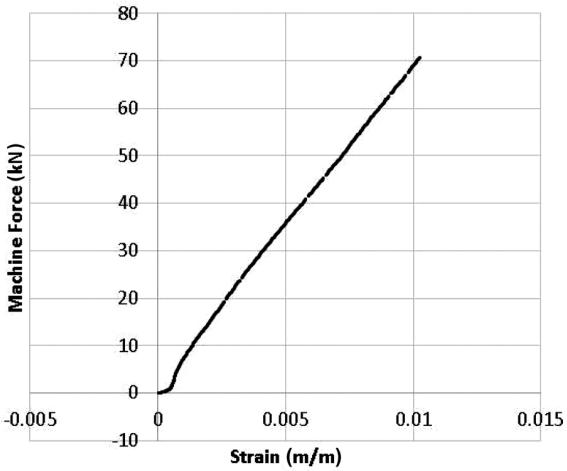

Fig. 13 Force–strain plot for CFC cylinder

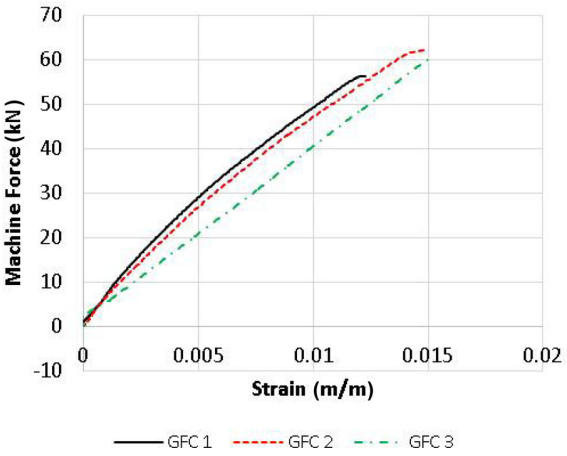

Fig. 14 Force–strain plot for GFC cylinders

fiber has the elastic modulus 230 GPa, Poisson's ratio 0.2, tensile strength 3530 MPa, and fracture strain 0.015 m/m. The epoxy has the elastic modulus 1.64 GPa and Poisson's ratio 0.33. The fiber volume fraction is 0.35, and the geometric data of the woven fabric have $a = 4$ mm, $b = 1.5$ mm, and $t = 0.25$ mm. Some of these data were measured while the others were obtained from the manufacturers.

The multiscale analysis was conducted as sketched in Fig. 6. The predicted elastic modulus of the CFC was 41.1 GPa, and the predicted strain at failure was 0.0128 m/m. These predicted results using the multiscale analysis agree very well with the tensile test data for CFC. The same multiscale analysis model was applied to the CFC cylinder. However, there were some unexpected variations in the CFC cylinder. The wall thicknesses of the CFC cylinders were not uniform since they were fabricated using hand lay-up. The average variation of the thickness was around 6% for the cylinders. That is, the thick side was 6% thicker than the thin side. A finite element simulation of a cylinder with a gradually varying thickness of 6% showed that the maximum hoop strain was 1.3 greater than the hoop strain of the cylinder with the uniform thickness. Considering the thickness variation, the failure hoop strain was 0.0098 m/m which agreed well with the experimental failure hoop strain of 0.010 m/m as shown in Fig. 13. Then, the experimental failure pressure computed using Eq. (3) was 12 MPa while the numerically predicted failure pressure was 13 MPa.

Three GFC cylinders were tested, and the test results were summarized in Table 5 and Fig. 14. The test data were quite consistent. The average internal pressure at failure is 11.0 MPa, and the average hoop strain on the outer surface of the cylinders is 0.0135 m/m, which corresponds to the failure hoop stress 240 MPa. The computed average elastic modulus of the GFC cylinders is 18.3 GPa.

The multiscale analysis technique was utilized to determine the elastic modulus of the GFC cylinder. The following constituent material properties were used: $E_f = 80$ GPa, $E_m = 1.64$ GPa, $\nu_f = 0.2$, and $\nu_m = 0.33$, where E and ν are the elastic modulus and Poisson's ratio, respectively, and subscripts f and m denote the fiber and matrix. The fiber volume fraction was 0.4. The plain weave architecture as shown in Fig. 8 had the geometric dimensions of $a = 4$ mm, $b = 2$ mm, and $t = 0.3$ mm. The predicted modulus from the multiscale analysis model was 18.4 MPa. As a result, the predicted stiffness of the GFC cylinder agreed very well with the experimental value.

Then, the failure strength of the GFC cylinder was also predicted using the multiscale analysis model. The average variation of the thickness was around 10% for the cylinders. A finite element simulation of the composite cylinder with the gradually varying thickness of 10% showed that the maximum hoop strain was 1.5 times greater than the uniform thickness cylinder. Considering the thickness variation, the failure hoop strain was 0.014 m/m, which agreed well with the experimental failure hoop strain of 0.015 m/m. Then, the experimental failure pressure computed using Eq. (3) was 10.0 MPa while the numerically predicted failure pressure was 11.5 MPa. Considering some uncontrolled misalignment of the fabric orientations in the cylinder, the agreement between the experimental and numerical results is acceptable.

Table 5 Glass-fiber composite calculated Young's modulus and burst pressure

	GFC #1	GFC #2	GFC #3	Average
Force (kN)	57.41	63.82	60.61	60.61
Experimental failure pressure[a] (MPa)	10.4	11.6	11.0	11.0
Elastic modulus (GPa)	18.8	16.0	20.2	18.3

[a]The pressure was computed from the force and the coefficient of friction using Eq. (3).

6 Conclusions

A mechanical device was developed and tested to determine the failure strength of a cylinder subjected to internal pressure loading. Uniaxial tensile equipment can be used to apply internal pressure loading without any fluid medium. Finite element analysis and experimental testing of aluminum alloy cylinders were conducted to assess the developed mechanical device. Both results confirmed the validity of the loading device. Then, the device was used to determine the failure strength and elastic modulus of the CFC and GFC cylinders. The test results were compared to the predicted results using a multiscale analysis model. The predictions agree well with the experimental data. The device is also planned to be used for composite cylinders fabricated using a filament-winding procedure, and the results will be also compared to the numerical results to be obtained using the multiscale analysis technique.

For the mechanical device to be effective, the initial gap between the device and the inner surface of the cylinder should be small. In addition, the cylinder should fail before the gaps among the wedges become too large.

Acknowledgment

The authors appreciate the assistance by Dr. C.-M. Park for helping with the experimental tests, and J. Mobley and J. Batteux for machining the experimental apparatus. Finally, we appreciate the financial support from Defense Threat Reduction Agency (DTRA).

References

[1] Onder, A., Sayman, O., Dogan, T., and Tarakcioglu, N., 2009, "Burst Failure Load of Composite Pressure Vessels," Compos. Struct., **89**(1), pp. 159–166.

[2] Xia, M., Takayanagi, H., and Kemmochi, K., 2001, "Analysis of Multi-Layered Filament-Wound Composite Pipes Under Internal Pressure," Compos. Struct., **53**(4), pp. 483–491.

[3] Xing, J., Geng, P., and Yang, T., 2015, "Stress and Deformation of Multiple Winding Angle Hybrid Filament-Wound Thick Cylinder Under Axial Loading and Internal and External Pressure," Compos. Struct., **131**(4), pp. 868–877.

[4] Hwang, T., Park, J., and Kim, H., 2012, "Evaluation of Fiber Material Properties in Filament-Wound Composite Pressure Vessels," Composites: Part A, **43**(9), pp. 1467–1475.

[5] Horide, A., Wakayama, S., and Kawahara, M., 1999, "Characterization of Fracture Process During Ring Burst Test of FW-FRP Composites With Damage," Adv. Compos. Mater., **8**(2), pp. 139–151.

[6] Rigaud, P., 2013, "Test Machine to Apply a Uniform Internal Pressure to a Tube," U.S. Patent No. 8,353,217 B2.

[7] Brovold, E., and Buttlar, W., 2001, "Compact Hollow Cylinder Tensile Tester," U.S. Patent No. 20,010,037,687 A1.

[8] Fleischlauer, E., 1962, "Pressure Fluid Ram," U.S. Patent No. 3044289 A.

[9] Kwon, Y. W., 2016, *Multiphysics and Multiscale Modeling: Techniques and Applications*, CRC Press, Boca Raton, FL.

[10] Kwon, Y. W., 2001, "Multi-Level Approach for Failure in Woven Fabric Composites," Adv. Eng. Mater., **3**(9), pp. 713–717.

[11] Kwon, Y. W., and Altekin, A., 2002, "Multi-Level, Micro-Macro Approach for Analysis of Woven Fabric Composites," J. Compos. Mater., **36**(8), pp. 1005–1022.

[12] Kwon, Y. W., and Park, M. S., 2013, "Versatile Micromechanics Model for Multiscale Analysis of Composite Structures," Appl. Compos. Mater., **20**(4), pp. 673–692.

[13] Park, M. S., and Kwon, Y. W., 2013, "Elastoplastic Micromechanics Model for Multiscale Analysis of Metal Matrix Composite Structures," Comput. Struct., **123**, pp. 28–38.